Key Points:
- The new TEX_{86} record suggests an impact of the Eurasian Ice Sheet dynamics on the Black Sea surface temperatures
- Orbital-scale temperature cooling is related to meltwater discharge
- Regional temperature records point to millennial-scale climate variability in the North Atlantic and Eurasia during the first half of MIS 6

Correspondence to:
A. Wegwerth,
antje.wegwerth@io-warnemuende.de

Impact of Eurasian Ice Sheet and North Atlantic Climate Dynamics on Black Sea Temperature Variability During the Penultimate Glacial (MIS 6, 130–184 ka BP)

Antje Wegwerth[1] , Jérôme Kaiser[1], Olaf Dellwig[1], and Helge W. Arz[1]

[1]Department of Marine Geology, Leibniz Institute for Baltic Sea Research Warnemünde (IOW), Rostock, Germany

Abstract Understanding hemisphere-wide millennial-scale temperature variability during past glacials in response to ice sheet dynamics and orbital forcing is one of the key targets for Quaternary climate research. While an inland propagation of abrupt temperature changes into Eurasia from the North Atlantic realm during the last glacial (Weichselian) receives increasingly broad support, much less is known regarding the penultimate glacial (Saalian) temperature variability, especially from a continental interior perspective. Here, we present a TEX_{86}-derived lake surface temperature (LST) record from the former Black Sea "Lake" covering nearly the entire Marine Isotope Stage (MIS) 6. While orbital-scale LST cooling likely relates to meltwater discharge from the retreating Eurasian Ice Sheet during insolation maxima, millennial-scale LST variability suggests interstadial warming in phase with Greenland and northern Mediterranean Sea temperature records during the first half of MIS 6. Although summer insolation reached an interglacial-like level during this period, we propose that the reduced extent of the Eurasian Ice Sheet associated with northward shifted atmospheric fronts was ultimately responsible for the inland propagation of Dansgaard-Oeschger-like temperature variability. During the second half of MIS 6, temperature patterns across the North Atlantic-Eurasian corridor were more variable and less comparable with each other, likely because of the larger continental ice sheet weakening northern hemisphere atmospheric teleconnections. Temperature records across the North Atlantic-Eurasian realm suggest a weaker atmospheric teleconnection during MIS 6 compared to MIS 3, likely related to a stronger imprint of the Eurasian Ice Sheet on the continental and regional climate.

1. Introduction

Marine Isotope Stage 6 (MIS 6; 191–130 ka BP; Lisiecki & Raymo, 2005) represents the latest period of the penultimate glacial (Saalian glaciation) that was one of the largest glaciations during the Quaternary characterized, by a 56% larger continental ice sheet compared to the last Weichselian glaciation (Batchelor et al., 2019; Colleoni et al., 2009; Hughes & Gibbard, 2018; Margari et al., 2014). The maximum Eurasian Ice Sheet (EIS) thickness during the Saalian exceeded the Weichselian one by 1,500 m (Lambeck, 1996; Lambeck et al., 2006). With the most southern ice sheet component, the Dnieper lobe, the Saalian ice sheet extended much deeper into the continental interior associated with a southward shifted atmospheric polar front (Figure 1; Colleoni et al., 2016; Ehlers & Gibbard, 2007; Hughes & Gibbard, 2018; Marks et al., 2018; Svendsen et al., 2004).

There is strong evidence for pronounced millennial-scale temperature variability during MIS 3, not only at the iconic sites from the North Atlantic and Greenland (e.g., Bond et al., 1993; Dansgaard et al., 1993; Martrat et al., 2007; McManus et al., 1999) but also from the Eurasian continental interior including the Black Sea, confirming a deep inland propagation of temperature anomalies through atmospheric teleconnections (e.g., Fleitmann et al., 2009; Tzedakis et al., 2004; Wegwerth et al., 2015). In contrast to stadial-interstadial temperature changes during the so-called Dansgaard-Oeschger (DO) cycles, the extra cooling during Heinrich stadials was most likely restricted to the eastern midlatitude North Atlantic (e.g., Ganopolski & Rahmstorf, 2001; Martrat et al., 2007). This was explained by a substantially weakened or complete shutdown of the Atlantic Meridional Overturning Circulation (AMOC) associated with a reduced northward ocean heat transport (Ganopolski & Rahmstorf, 2001; Van Meerbeeck et al., 2011; Zhang et al., 2014).
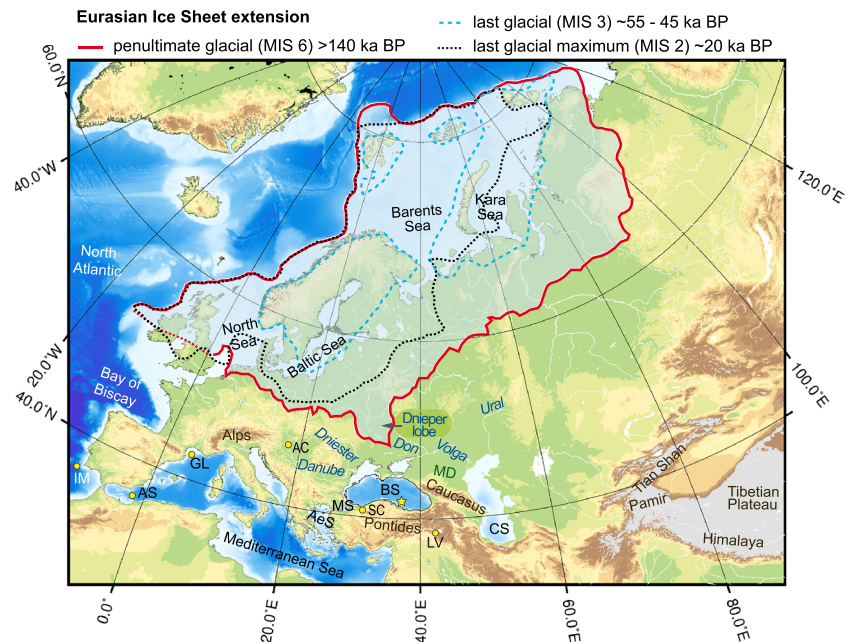
Figure 1. Map showing Eurasia and the Black Sea with core site of MSM 33 (yellow star), regions discussed in the text (yellow circles), and the maximum extent of the Eurasian Ice Sheet during the Saalian (MIS 6; modified from Svendsen et al., 2004) and Weichselian (MIS 2 and 3; modified from Larsen et al., 2006). AC = Abaliget Cave; AeS = Aegean Sea; AS = Alboran Sea; BS = Black Sea; CS = Caspian Sea; GL = Gulf of Lions; IM = Iberian Margin; LV = Lake Van; MD = Manych Depression; MS = Marmara Sea; SC = Sofular Cave. Map modified from Wegwerth et al. (2019).

During MIS 6, millennial-scale temperature variability affected climate patterns in Greenland, the midlatitude North Atlantic, and the Western Mediterranean Sea (e.g., Barker et al., 2011; Cortina et al., 2015; Margari et al., 2014; Martrat et al., 2004; Martrat et al., 2007). The synthetic δ^{18}O Greenland record derived from the Antarctic ice core record suggests, for example, large amplitude temperature changes particularly between 180 and 160 ka BP attributed to an intermediate climate state comparable to MIS 3 (Barker et al., 2011). For the North Atlantic and Western Mediterranean Sea, alkenone-based temperature reconstructions show DO-like temperature changes with amplitudes similar to MIS 3 (Martrat et al., 2004; Martrat et al., 2007). However, the temperature history of the Eurasian interior is largely unknown for the penultimate glacial, when orbital setting and ice sheet configuration were substantially different. Apart from the larger EIS extent during MIS 6, orbital cycles fluctuated on a higher amplitude resulting in an interglacial-like northern hemisphere summer insolation (NHSI; Berger & Loutre, 1991). Quantitative temperature reconstructions are sparse for continental southern Europe during the entire MIS 6 (Sinopoli et al., 2019; Wainer et al., 2013). A stable isotope flowstone record from SW France covering the early MIS 6 documents five stadial-interstadial cycles between 177 and 165 ka BP (Wainer et al., 2013). Likewise, palynological reconstructions from north-western Greece suggest at least millennial-scale temperature variations between 185 and 155 ka BP with frequent warm periods and thereafter even colder conditions than during MIS 3 (Roucoux et al., 2011). For the second half of MIS 6 pollen data suggest strong cooling followed by a warmer phase toward the Eemian interglacial (Sinopoli et al., 2019). A long continuous pollen record from Lake Padul at the southern Iberian Peninsula covering the last two glacial-interglacial cycles mainly reveals orbital-scale changes in vegetation forced by insolation with a striking warmer period between 178 and 168 ka BP (Camuera et al., 2018, 2019). Most recently, Rousseau et al. (2020) documented DO-like cycles during MIS 6 for the Bulgarian Harletz loess sequence as reflected by alternation between paleosol and loess with the first representing warmer and more humid interstadials. Although less obvious than during the last glacial (MIS 4–2), μ-XRF Ca oscillations observed in a new sedimentary sequence from the Sea of Marmara covering the last 171 kyr suggest stadial-interstadial variability during MIS 6 (Çağatay et al., 2019). Despite these data, high-resolution quantitative temperature reconstructions for the Eurasian continent during the entire MIS 6 are missing.
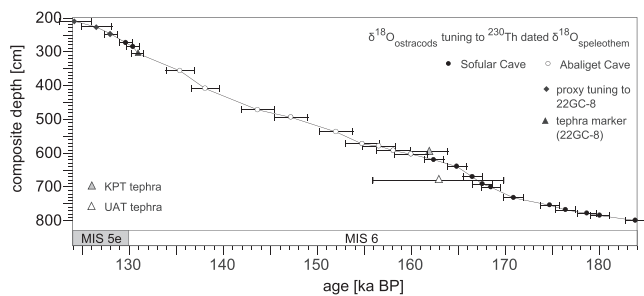
Figure 2. Age-depth model of the composite core from the Black Sea between 184 and 124 ka BP. KPT = Kos Plateau Tuff; UAT = Upper Acigöl Tuff (from Wegwerth et al., 2019).

To test the effect of the different boundary conditions on climate variability on the Eurasian continent during MIS 6 and MIS 3, we have reconstructed surface water temperature by means of the TEX_{86} (TetraEther IndeX of lipids with 86 carbon atoms; Schouten et al., 2013) paleothermometer from a composite sediment core covering the penultimate glacial phase of the former SE Black Sea "Lake." We further included the content of coastal ice-rafted detritus (IRD_C), which has been proven a further valuable - temperature-related proxy (Nowaczyk et al., 2012; Wegwerth et al., 2014, 2015, 2019).

2. Materials and Methods

2.1. Sediment Cores and Chronology

This study is based on a composite core recovered from the Archangelsky Ridge in the SE Black Sea during RV Maria S. Merian cruise MSM33 in 2013 (Figure 1; Arz et al., 2014). The composite core (MSM33, 593 cm length) comprises three gravity cores (MSM33/60-1GC, MSM33/57-1GC, and MSM33/56-1GC) derived from about the same location at water depths ranging between 374 and 499 m. The age model of the composite core primarily bases on fine-tuning of the Black Sea $\delta^{18}O_{ostracods}$ record (Figure 2; Wegwerth et al., 2019) to $\delta^{18}O$ records of ^{230}Th dated speleothems from Northern Anatolia and Hungary (Badertscher et al., 2011; Koltai et al., 2017). Additionally, the Kos Plateau Tuff (KPT, 161 ± 2 ka; Bachmann et al., 2010; Smith et al., 1996) and the Upper Acigöl Tuff (UAT; 163 ± 7 ka, Schmitt et al., 2011) assisted as tephra markers that confirmed the stratigraphy. The composite core covers almost the entire MIS 6 (130–184 ka BP), which corresponds in the Black Sea to the climatostratigraphic unit Geroevskoe II within the middle part of the Karangatian (300–50 ka BP) (Zubakov, 1988). Relative high mean sedimentation rates of 12 cm/kyr allowed reconstructing the paleotemperature variability with a mean resolution of 0.3 kyr.

2.2. Sample Preparation and GDGTs Analysis

In total 180 samples taken every 3–4 cm were analyzed for glycerol dialkyl glycerol tetraethers (GDGTs). The method for lipid extraction and separation has been previously described in Kaiser and Arz (2016). The sample preparation involved accelerated solvent extraction (Thermo Scientific™ Dionex™ ASE™ 350) of previously freeze-dried and homogenized sediments (4–6 g) with a mixture of dichloromethane and methanol (DCM/MeOH 9:1, v:v). The isolation of the polar fraction containing the GDGTs was done using column chromatography in a Pasteur pipette plugged with activated Al_2O_3 and a DCM/MeOH (1:1, v:v) mixture as eluent. After the addition of a C46 GDGT internal standard for quantification and the filtration of the fractions through a 0.45 μm polytetrafluoroethylene filter, GDGTs were analyzed by high performance liquid chromatography atmospheric pressure chemical ionization mass spectrometry (HPLC APCI-MS) as described in Kaiser and Arz (2016) except for a small modification. Following Hopmans et al. (2016), the separation of the individual GDGTs was achieved on two UHPLC silica columns (BEH HILIC, 2.1 mm × 150 mm, 1.7 μm; WatersTM) in series, fitted with a pre-column of the same material (WatersTM), and maintained at 30°C. Using a flow rate of 0.2 ml/min, the gradient of the mobile phase was first held isocratic for 25 min with 18% solvent B (n-hexane:isopropanol, 9:1, v:v) and 82% solvent A (n-hexane), followed by a linear gradient to 35% solvent B in 25 min, followed by a linear gradient to 100% solvent B in 30 min. The column was further equilibrated with 18% solvent B for 20 min before the next run. Peaks were identified by single-ion monitoring (SIM) at m/z 1,021.6–1,022.4 (GDGT-Ia), 1,035.6–1,036.4 ($GDGT-II_{5Me}$), 1,049.6–1,050.4 ($GDGT-III_{5Me}$), 1,291.9–1,292.7 (cren and cren′), 1,295.9–1,296.7 (GDGT-3), 1,297.9–1,298.7 (GDGT-2), 1,299.9–1,300.7 (GDGT-1), and 1,301.9–1,302.7 (GDGT-0). The global lake calibration with error bars of ±3.7°C (Powers et al., 2010) was used to convert the TEX_{86} values into mean annual lake surface temperature (LST) estimates. The mean standard deviation of measurements of an in-house TEX_{86} standard was 0.008 (0.4°C, with the calibration of Powers et al., 2010; n = 16). The TEX_{86} is expected to mirror mean near-surface annual temperatures during the glacial stages of the Black Sea (Wegwerth et al., 2014; Wegwerth et al., 2015). The Branched and Isoprenoid Tetraether (BIT) index represents the relative abundance of terrestrial tetraether lipids to crenarchaeol and was calculated according to Hopmans et al. (2004). The methane index (MI) was used for
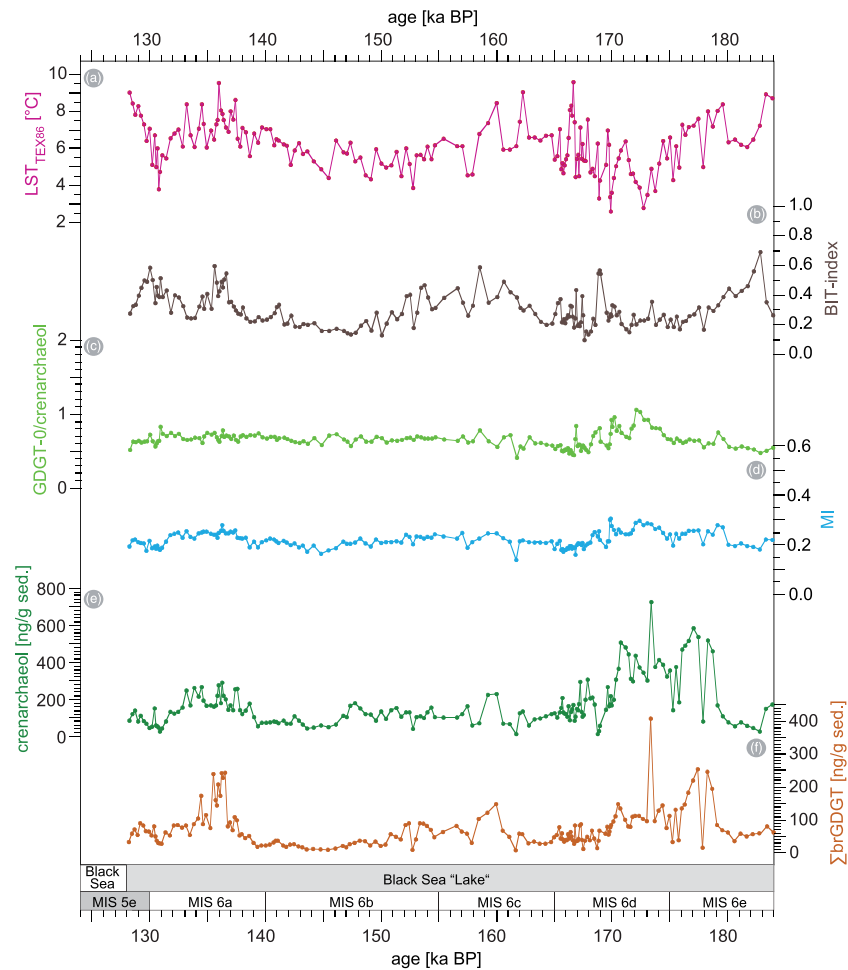
Figure 3. Organic proxies in the Black Sea during MIS 6: (a) the TEX_{86}-based lake surface temperature (LST; after Powers et al., 2010), (b) the Branched and Isoprenoid Tetraether (BIT) index = (GDGT-Ia + GDGT-II$_{5Me}$ + GDGT-III$_{5Me}$)/(cren + GDGT-Ia + GDGT-II$_{5Me}$ + GDGT-III$_{5Me}$) (Hopmans et al., 2004), (c) the GDGT-0/crenarchaeol ratio, (d) the methane index (MI) = (GDGT-1 + GDGT-2 + GDGT-3)/(GDGT-1 + GDGT-2 + GDGT-3 + cren + cren′) (Zhang et al., 2011), (e) the sedimentary content of crenarchaeol, and (f) the sum of brGDGTs.

estimating the potential influence of isoprenoid GDGTs produced by methanotrophic *Euryarchaeota* on the TEX_{86} index (Zhang et al., 2011).

2.3. Northern Hemisphere Temperature Records Covering MIS 3 and MIS 6

To assess the importance of the different orbital setting and the ice sheet configuration for atmospheric teleconnection and temperature patterns during the last two glacial periods MIS 6 and MIS 3, we have compared the $\delta^{18}O_{synth.}$ Greenland record with available paleotemperature records in the North Atlantic-Eurasian region and the Black Sea "Lake" record (MIS 3: Wegwerth et al., 2015; MIS 6: this study). Included study sites are Lake Van (Anatolia; Ön & Özeren, 2018), the Gulf of Lions (NW Mediterranean Sea; Cortina et al., 2015), the Alboran Sea (Western Mediterranean Sea; Martrat et al., 2004), and the Iberian Margin (eastern North Atlantic; Margari et al., 2014; Martrat et al., 2007). The records from the Mediterranean Sea and the North Atlantic are alkenone-based sea surface temperatures (SSTs), whereas data from the Gulf of Lions represent spring-winter SST and the remaining spring-summer conditions (Cortina et al., 2015; Margari et al., 2014; Martrat et al., 2004; Martrat et al., 2007). The Lake Van record bases on an independent component analysis (Ön & Özeren, 2018) of various data comprising, for example, XRF element intensities of Ca, Fe, K, Mn, and Si, as well as TOC, CaCO$_3$, and color reflectance (Kwiecien et al., 2014; Stockhecke et al., 2014, 2016), and
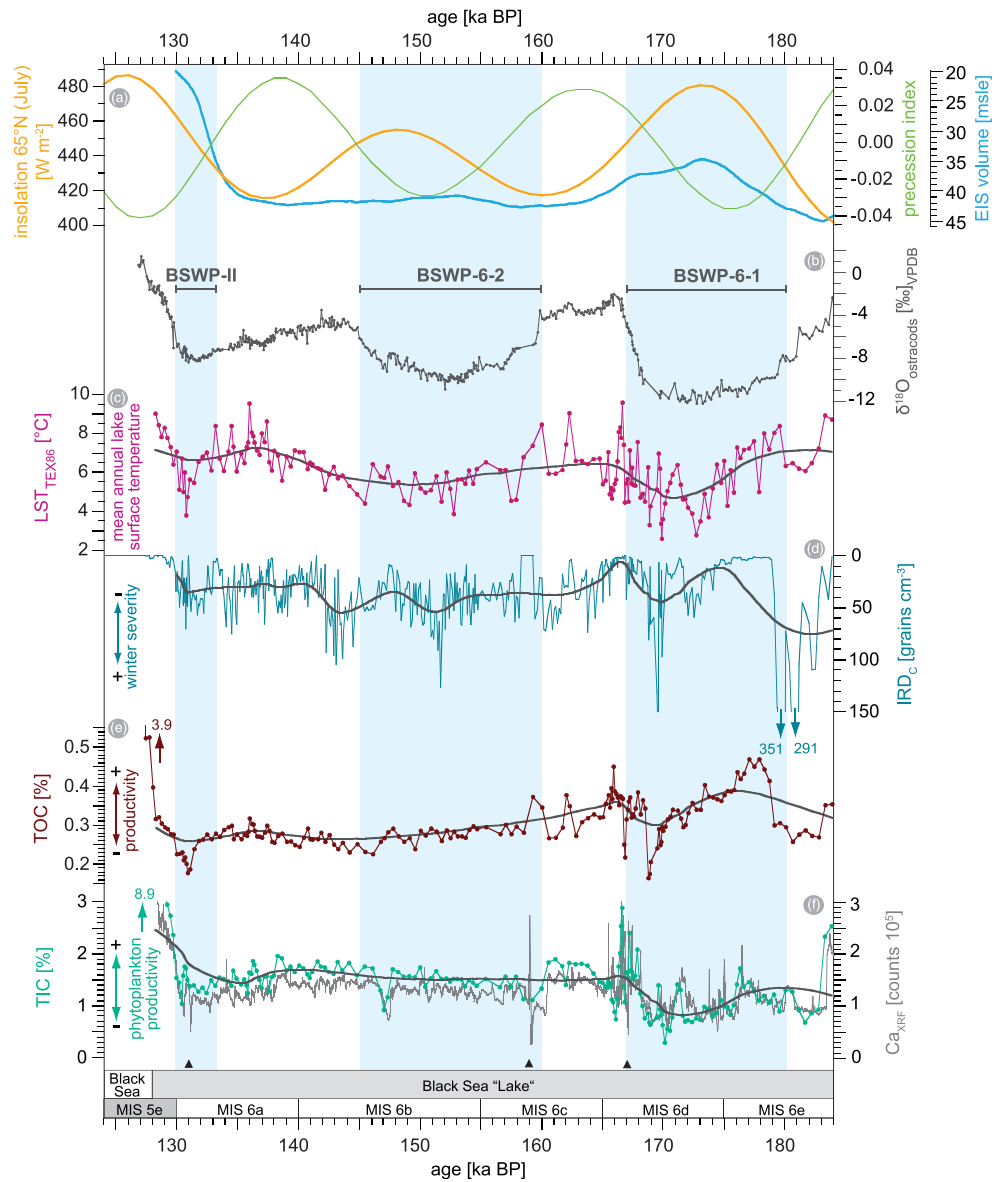
Figure 4. Climate conditions in the Black Sea "Lake" during Marine Isotope Stage 6 (184–130 ka BP). (a) Orbital parameters of insolation and precession (Berger & Loutre, 1991) and the Eurasian Ice Sheet (EIS) volume relative to present (msle = m sea level equivalent; note reversed scale; Bintanja & van de Wal, 2008); (b) $\delta^{18}O_{ostracods}$ record from the Black Sea reflecting Black Sea water pulses (BSWP; blue shaded); (c) TEX$_{86}$-based mean annual lake surface temperature (LST); (d) number of coastal ice-rafted detritus (IRD$_C$); reversed scale; (e) total organic carbon (TOC); (f) total inorganic carbon (TIC) and Ca XRF-counts. Gray solid lines in (c)–(f) indicate long-term trends obtained by fast Fourier transformation with cutoff frequencies at 0.107 (c, e, f) and 0.245 (d). (b) and (d)–(f) from Wegwerth et al. (2019). Triangles indicate tephra layers (Wegwerth et al., 2019).

thus reflects qualitatively warming and cooling without a quantitative temperature reconstruction. Although the average resolution of 7 kyr of an alkenone-based U$^K_{37}$ record from an additional study of Lake Van (Randlett et al., 2014) during MIS 6 limits the comparison with the other temperature data sets used here, we added it to the independent component analysis data as temperature estimates. For better comparison between the individual MIS 6 records, we modified the age model for the SST record from the Alboran Sea by tuning the $\delta^{18}O_{planktonic}$ record from the Alboran Sea to the already age model-corrected $\delta^{18}O_{planktonic}$ record from the North Atlantic (Supporting Information Figure S1; Margari et al., 2010, 2014; Martrat et al., 2004).
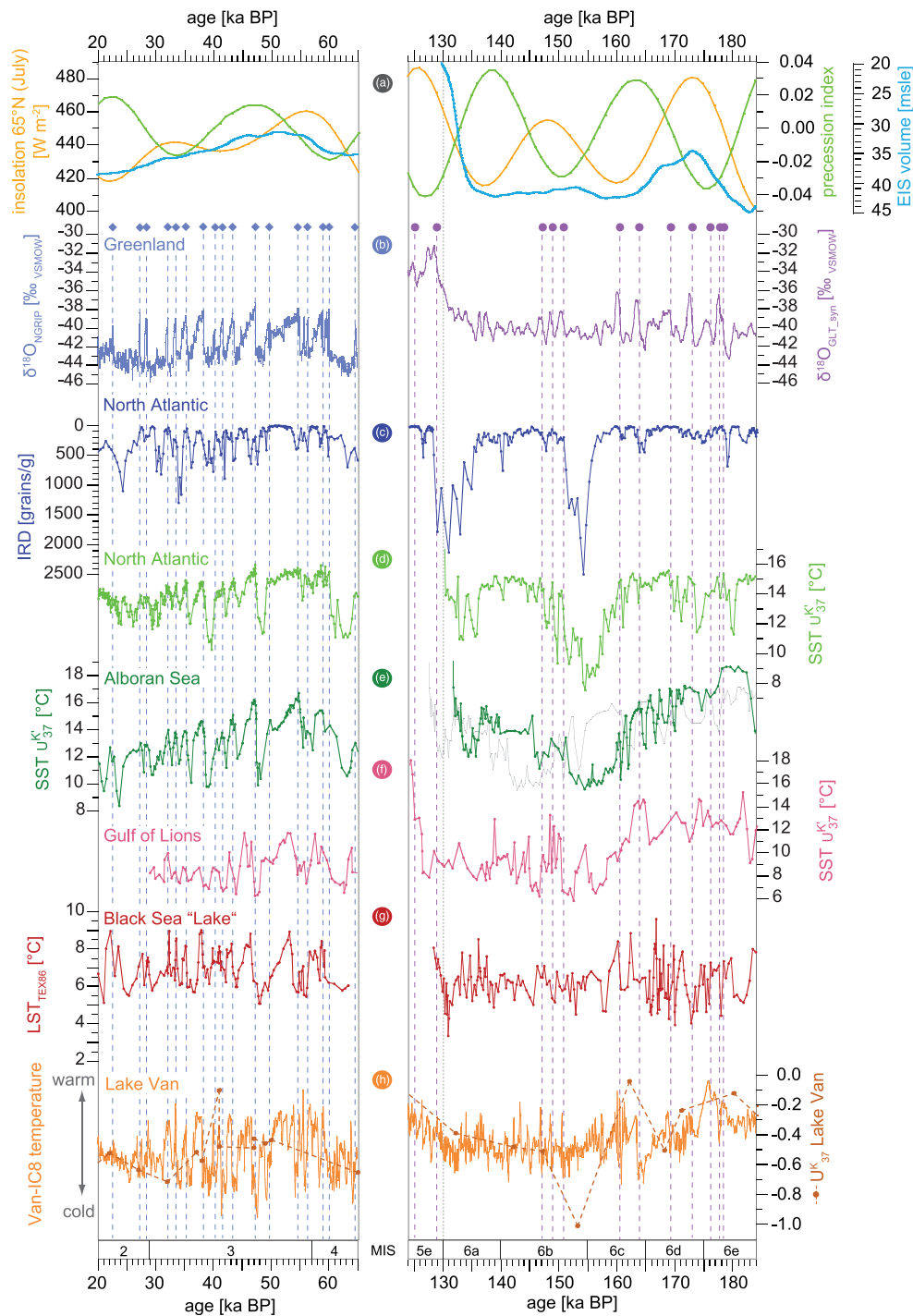
Figure 5. Temperature conditions during the last two glacials (MIS = Marine Isotope Stages 6–5e and 4–2). (a) Orbital parameters of northern hemisphere summer insolation and precession (Berger & Loutre, 1991) and the Eurasian Ice Sheet (EIS) volume relative to present (msle = m sea level equivalent; note reversed scale; Bintanja & van de Wal, 2008); (b) $\delta^{18}O$ variations of a Greenland ice core with filled circles and vertical dashed lines representing predicted DO events proposed by Barker et al. (2011); blue = core NGRIP with filled diamonds and vertical dashed lines representing DO events (North Greenland Ice Core Project members, 2004); violet = synthetic Greenland core (Barker et al., 2011, speleo-age timescale); (c) number of ice-rafted detritus (IRD) from the northern North Atlantic (reversed scale, Barker et al., 2015); (d) alkenone-based sea surface temperature (SST) from the North Atlantic/Iberian Margin (Margari et al., 2014; Martrat et al., 2007); (e) alkenone-based sea surface temperature (SST) from the Alboran Sea (Western Mediterranean Sea; Martrat et al., 2004; MIS 6: gray = original; green = modified age model; see Supporting Information); (f) alkenone-based sea surface temperature (SST) from the Gulf of Lions (NW Mediterranean Sea; Cortina et al., 2015); (g) TEX_{86}-based mean annual lake surface temperature in the Black Sea "Lake" (LST, last glacial LST from Wegwerth et al., 2015); MIS 6: detrended LST (this study); and (h) temperature estimations for Lake Van based on independent component analysis (ICA) of various data from the lake (Ön & Özeren, 2018, and references therein) and alkenone-based U^{K}_{37} index for estimations of warming and cooling (Randlett et al., 2014).

3. Results

The TEX_{86} mean annual LST record in the Black Sea during MIS 6 ranges between 2.6°C and 9.6°C (mean of 6°C; Figure 3a). The largest amplitudes of LST occur during the periods 184–160 and 145–130 ka BP. Pronounced millennial-scale temperature variability is superimposed to the long-term trend, which shows lower values during NHSI maxima (Figures 4a and 4c). Coldest conditions occurred around 173, 153, and 131 ka BP. For a more suitable estimation of the temperature changes on a millennial timescale, we removed the orbital-scale long-term pattern by applying a Savitzky-Golay filter (Savitzky & Golay, 1964) and added the average LST to the resultant temperature deviation (Figure 5g). The resultant record reveals largest amplitudes along with more frequent warmer conditions until 160 ka BP.

4. Discussion

4.1. Reliability of the TEX_{86} Temperature Proxy in the Glacial Black Sea "Lake"

Although TEX_{86} can be biased by different factors not related to water temperature, previous studies have shown that the proxy reflects LST changes during former limnic stages of the Black Sea (Ménot & Bard, 2012; Soulet et al., 2011; Wegwerth et al., 2014, 2015). In the present MIS 6 record, the relatively low BIT index with a mean value of 0.3 ± 0.1 (mean and standard deviation values; Figure 3b) excludes a significant input of soil-derived isoprenoid GDGTs that may biased the TEX_{86} values for most of the record (Castañeda & Schouten, 2011; Hopmans et al., 2004; Weijers et al., 2006). However, some individual outliers occurring at 183–180, 169, 161–159, 157, 154, 152, 137–135, and 131–129 ka BP have BIT values >0.4, which may relate to an enhanced contribution by terrestrial GDGTs potentially biasing TEX_{86} values. However, it has been shown that the BIT index may not always be a suitable proxy for terrestrial input (Fietz et al., 2011; Schmidt et al., 2010; Smith et al., 2012). Indeed, the similar pattern of crenarchaeol and brGDGTs concentrations ($n = 180$, $r^2 = 0.55$, $p < 0.01$; Figures 3e and 3f) suggests mostly an in situ production of brGDGTs and not a terrestrial origin. By contrast, the patterns of the BIT index and brGDGTs share less similarities ($n = 180$, $r^2 = 0.11$, $p < 0.01$; Figures 3b and 3f). Similarly, TEX_{86} shows a relation neither to BIT ($n = 180$, $r^2 = 0.05$, $p < 0.01$) nor to MI ($n = 180$, $r^2 < 0.01$, $p = 0.80$; Figure 3). Therefore, we consider no significant impact of terrestrial GDGTs on the TEX_{86} paleothermometer record of the glacial Black Sea "Lake."

Furthermore, the permanent presence of benthic ostracods, low contents of total organic carbon, and lack of enrichment of redox-sensitive trace metals during MIS 3 and MIS 6 strongly suggest that the Black Sea water column was not affected by oxygen deficiency or methanogenic activity, which could have impacted habitat depths and/or phylogeny of the archaeal community and potentially biased TEX_{86} values (Hurley et al., 2016; Kusch et al., 2016; Qin et al., 2015; Wegwerth et al., 2014, 2016, 2018, 2019). This is further evidenced by a GDGT-0/crenarchaeol mean ratio <2 (0.6 ± 0.1; Figure 3c), which is typical for *Thaumarchaeota* and further suggests that methanogens are negligible as additional source of isoprenoid GDGTs (Blaga et al., 2009; Schouten et al., 2002, 2013; Turich et al., 2007). As well, the mean value of the MI (0.2 ± 0.03; Figure 3d; Zhang et al., 2011) suggests that the contribution of isoprenoid GDGTs produced by methanotrophic *Euryarchaeota* was low enough to not bias the TEX_{86} temperatures. Considering all these evidences, TEX_{86} is very likely a suitable temperature proxy for the Black Sea surface water during MIS 6, as well as during MIS 3 (Wegwerth et al., 2014, 2015).

4.2. Orbital-Scale Temperature Trends in the Black Sea "Lake" During MIS 6

The long-term TEX_{86}-based LST pattern in the Black Sea "Lake" record during MIS 6 resembles both the pattern of orbital configuration and that of the EIS volume (Figures 4a and 4c; Berger & Loutre, 1991; Bintanja & van de Wal, 2008; Laskar et al., 2004). During NHSI maxima, a retreated EIS suggests generally milder conditions (Figure 4a; Berger & Loutre, 1991; Bintanja & van de Wal, 2008; Laskar et al., 2004). However, unlike as might be expected, the Black Sea LST indicates colder conditions during these periods. At ~173 ka BP, that is, when insolation was on an interglacial-like maximum and EIS volume was on a minimum level, the LST dropped by up to 2.6°C and were more than 2°C lower compared to MIS 3 minimum values (Figures 5a and 5g; Wegwerth et al., 2015).

There are three cooling periods centered at 173, 153, and 131 ka BP, and the first was the coldest period. Nevertheless, these three periods coincide with a smaller EIS volume (Figures 4a and 4c; Bintanja & van

de Wal, 2008) and were most likely affected by long-lasting meltwater discharge into the Black Sea "Lake" (Badertscher et al., 2011; Shumilovskikh et al., 2013; Wegwerth et al., 2014, 2019). The pronounced negative excursions of $\delta^{18}O$ of benthic ostracods in these periods suggest an input of cold freshwater with an isotopically lighter signature (Figure 4b; Shumilovskikh et al., 2013; Wegwerth et al., 2014, 2019). Therefore, the long-term LST cooling episodes during the insolation maxima likely reflect the thermal impact of the meltwater derived from the disintegrating EIS directly and via the Caspian detour (Wegwerth et al., 2019).

Previously, it has been shown that the abundance of coastal IRD_C in glacial sediments of the Black Sea reflect winter severity (Nowaczyk et al., 2012; Wegwerth et al., 2015, 2019). The IRD_C record during MIS 6 (Wegwerth et al., 2019) resembles the LST pattern and suggests stronger winters during periods of lower annual mean LST. This is mostly true for both the individual IRD_C and LST data points and the reconstructed long-term trends (solid gray lines, Figures 4c and 4d) with a clear exception during 184–178 ka BP. The diverging long-term trends can be explained by the larger variability and amplitude in the IRD_C record that likely impacts the trend more strongly compared to the LST, with the latter being also most likely overprinted by meltwater as discussed above. The complete absence of frequent IRD_C during the first half of MIS 6 implies ice-free conditions and significantly milder winters at the southern coast of the Black Sea (Figures 4c and 4d) during a period of generally increased insolation and a retreated EIS. Thus, despite a possible overprint by meltwater, the IRD_C and LST records suggest warmer conditions during the first part of MIS 6 (180–160 ka BP). Such warmer conditions likely favored a slightly increased primary productivity in the Black Sea "Lake" as seen by higher sedimentary contents of TOC (Figure 4e; Wegwerth et al., 2019). This relationship has already been described for the MIS 3 Black Sea "Lake" sediments (Wegwerth et al., 2016).

The warmer period during the first half of MIS 6 in the Black Sea coincides with the formation of the so-called cold sapropel S6 in the Mediterranean Sea (Bard et al., 2002; Rohling et al., 2015; Schmiedl et al., 2003). It further corresponds to a warmer and wetter phase in the entire Mediterranean Sea, as indicated by increased arboreal pollen and alkenone-based SSTs, as well as a pronounced $\delta^{18}O$ excursion in speleothems (Bard et al., 2002; Emeis et al., 2003; Tzedakis et al., 2003).

The second half of MIS 6 shows generally colder conditions in temperature records from the North Atlantic toward the Black Sea (Figure 5; Cortina et al., 2015; Margari et al., 2014; Martrat et al., 2004, 2007; Ön & Özeren, 2018). Cold conditions in the northern North Atlantic are further confirmed by maximum IRD amounts at around 154 and 131 ka BP (Figure 5c; Barker et al., 2015). Else than during the first meltwater period in the Black Sea (BSWP-6-1), the partial retreat of the EIS concomitant to the second large MIS 6 meltwater phase (BSWP-6-2; 160–145 ka BP; Figures 4a and 4b) resulted in massive meltwater discharge into the North Atlantic (Toucanne et al., 2009). This may have triggered a weakened AMOC and pronounced cooling during the long-lasting 158–152 ka BP Heinrich stadial (Figures 5c and 5d; Barker et al., 2015; Boswell et al., 2019; Margari et al., 2014; Martrat et al., 2007; Penaud et al., 2009; Toucanne et al., 2009) that affected temperatures in the North Atlantic and the Mediterranean Sea and possibly also slightly in the Black Sea region.

In the context of weakened AMOC and temperatures, Cortina et al. (2015) pointed out that during the last glacial-interglacial cycles, SST in the Gulf of Lions were strongly driven by NHSI, whereas SST records from the Alboran Sea and Iberian Margin (Martrat et al., 2004, 2007) seem less affected by NHSI and are more related to AMOC variability. The authors further noted that the correspondence between SST in the Gulf of Lions and NHSI was lower during glacials (including MIS 6) because of a stronger influence of the EIS on the SST. In particular, during periods of increased ice extent and lower amplitude NHSI (such as during the second half of MIS 6), the intensity of northwesterly winds was higher and the atmospheric polar front migrated southward both resulting in colder conditions in the Gulf of Lions (Cortina et al., 2015). In this regard, the cooling episode in the Black Sea during Termination II at around 131 ka BP coinciding with the North Atlantic Heinrich stadial 11 likely reflects both a meltwater cooling impact and a cooling by the general northern hemisphere cold conditions due to a weakened AMOC transferred by the westerly winds to the continent interior. While we suggest that all three MIS 6 cooling periods were mainly caused by a regional meltwater input, we assume an additional cooling effect due to a weakened AMOC at least for the younger two periods of MIS 6 since these coincide with North Atlantic Heinrich stadials.

4.3. Millennial-Scale Temperature Variability in the Black Sea "Lake" During MIS 6

Both temperature-related records, that is, LST and IRD_C, from the Black Sea reflect warming and cooling that nearly coincide with DO events during MIS 6 as predicted from the Greenland synthetic $\delta^{18}O$ ice core record (Figures 4c, 4d, 5b, and 5g; Barker et al., 2011). The new Black Sea "Lake" LST detrended record (Figure 5g) is also consistent with DO-like temperature variability as recorded in the North Atlantic, the Western Mediterranean Sea, and the Anatolian Lake Van (Figures 5d–5h; Cortina et al., 2015; Margari et al., 2010, 2014; Martrat et al., 2004, 2007; Ön & Özeren, 2018). However, it has to be noted that the comparison of the temperature records covering MIS 6 is slightly hampered because of the different and large age uncertainties of the individual regional records reaching up to ± 4 kyr. For the Black Sea MIS 6 record, for example, mean squared estimates (MSEi) of age uncertainty determined after Grant et al. (2012) range between ± 0.7 and ± 1.8 kyr (Wegwerth et al., 2019). Similarly, the record from the North Atlantic (Margari et al., 2014) was aligned to the synthetic Greenland record (Barker et al., 2011), which in turn was tuned to the Chinese speleothem age scale showing age uncertainties of about 1.5 kyr for MIS 6 (Wang et al., 2008). The age model of the temperature record from the Gulf of Lions (Cortina et al., 2015) is based on tuning to the LR04 benthic stack (Lisiecki & Raymo, 2005) from which age uncertainties of up to ± 4 kyr were reported. Despite these age uncertainties, the similar temperature patterns suggest a close atmospheric teleconnection along the North Atlantic-Eurasian corridor during MIS 6. However, strong DO-like temperature variability in the Black Sea region during MIS 6 is somewhat puzzling, because the EIS was considerably larger and covered a much wider area into the continent compared to the last glacial (Figure 1; Colleoni et al., 2009; Colleoni et al., 2016; Hughes & Gibbard, 2018; Marks et al., 2018; Svendsen et al., 2004). While a smaller continental ice sheet resulted in an increased meridional atmospheric teleconnection across the North Atlantic and Eurasia, as for MIS 3, a larger ice sheet should weaken such connection by acting as a barrier for the westerly winds reducing the strength and/or deflecting the frontal systems southward (Feurdean et al., 2014; Pollard & Barron, 2003; Wegwerth et al., 2015).

However, similar to the synthetic $\delta^{18}O$ record for Greenland, the Black Sea stadial-interstadial temperature changes show higher amplitudes and frequencies along with more frequent warmer periods during the first half of MIS 6, which is probably associated with the higher NHSI and retreated EIS (Figures 5a, 5b, and 5g). Warmer interstadials during the first half of MIS 6 are also suggested by the Lake Van and the Mediterranean records. The SST pattern from the North Atlantic is lacking a typical stadial/interstadial pattern but reveals a few prominent stadial cooling events corroborated by an IRD record from the northern North Atlantic (Barker et al., 2015) (Figures 5c and 5d). The difference between the temperature records of the North Atlantic and the Mediterranean/Black Sea region may reflect different responses to atmospheric and oceanic forcing on temperature variability in the oceanic North Atlantic realm and over the Eurasian continent. The different regional MIS 6 temperature records suggest that sites close to the North Atlantic are more sensitive to cooling, whereas continental sites are rather sensitive to warming. Accordingly, millennial-scale North Atlantic SST minima during MIS 6 are likely related to an AMOC weakening, whereas the observed continental temperature patterns are more directly influenced by NHSI and especially by EIS dynamics (Cortina et al., 2015); these latter being two important factors controlling the atmospheric circulation patterns across Eurasia. Similar differences are evident also for MIS 3, where cooling events in the North Atlantic and the Western Mediterranean Sea are much more pronounced (Martrat et al., 2004, 2007) compared to the concomitant stadial SSTs at more continental sites (Figure 5; Cortina et al., 2015; Ön & Özeren, 2018; Wegwerth et al., 2015). An exception is the TEX_{86}-based temperature record from the western Black Sea during MIS 3 (Ménot & Bard, 2012), where interstadials are less obvious than cooling related to Heinrich stadials as discussed by Wegwerth et al. (2015). Although reconstructions show a generally much larger EIS extent into the Eurasian interior during MIS 6 (Colleoni et al., 2009, 2016; Hughes & Gibbard, 2018; Marks et al., 2018; Svendsen et al., 2004), the almost exclusive occurrence of DOs across the North Atlantic-Eurasian corridor during the first part of MIS 6 potentially benefited from the interglacial-like NHSI maximum and a pronounced northward waning of the continental EIS to a volume comparable to the early MIS 3.

The bundled DO successions separated by pronounced Heinrich stadial cooling in MIS 3 (Bond et al., 1993; Heinrich, 1988), the so-called Bond cycles, are not evident during MIS 6, and the timing and nature of the DO-like temperature changes is more variable between the various records. One reason is most likely the

larger uncertainties of the individual age models compared to the partly radiocarbon dated MIS 3 records. Another reason is probably related to the stronger regional impact of the large amplitude changes in NHSI and the EIS volume. Lower amplitudes during MIS 3 probably favored a stronger zonal atmospheric teleconnection across the North Atlantic-Eurasian corridor causing less regional differences and a stronger imprint of northern hemisphere climate in general (Wegwerth et al., 2015, 2016).

During the insolation maximum within MIS 3, all regional temperature records show DO interstadials being generally longer in duration than interstadials during lower insolation (Figure 5). The insolation maximum at ~55 ka BP during MIS 3 is comparable with the second insolation maximum during MIS 6 at ~148 ka BP. Although Barker et al. (2011) predicted at least two interstadials during the second insolation maximum within MIS 6 for Greenland (Figure 5b), the individual temperature patterns across the North Atlantic-Eurasian corridor are less clear and show shorter interstadials (Figure 5). A much larger volume and areal extent of the EIS during the middle part of MIS 6 (Figure 5a) may explain the considerably different temperature patterns compared to MIS 3. However, during the first and more pronounced insolation maximum within MIS 6 at ~173 ka BP, the EIS was reduced considerably to a volume comparable to that at ~55 ka BP (Figure 5a; Bintanja & van de Wal, 2008). Therefore, the retreated ice sheet associated with a northward migration of the atmospheric polar front and the subtropical jet likely caused the generally milder conditions in the midlatitudes. After a short cooling during Heinrich stadial 11, all compared temperature records show pronounced warming since ca. 130 ka BP (Figure 5) most likely related to the final retreat of the EIS at the penultimate glacial-interglacial transition (Termination II), allowing again a deeper inland propagation of the milder North Atlantic climate.

5. Conclusions

The TEX$_{86}$-based surface temperature record from the Black Sea "Lake" covering nearly the entire MIS 6 documents pronounced temperature variability on an orbital and millennial scale. Else than expected, temperatures are lower during NHSI maxima, which is most likely related to the long-lasting discharge of colder meltwater into the Black Sea "Lake" from the retreating EIS during these periods. Removing this long-term trend, the temperature-related LST and IRD$_C$ proxy records clearly point to millennial-scale variability coinciding, within the uncertainty of dating, with predicted Greenland DO cycles particularly during the first part of MIS 6. After ~160 ka BP, the Black Sea was more "locked" in a stable colder condition due to the expansion of the EIS and the southward migration of the atmospheric polar front over the Black Sea region. During the first half of MIS 6, temperature records from the North Atlantic, the Mediterranean Sea, and the Black Sea region share common millennial-scale features with stadial cooling and interstadial warming most likely favored by a retreated EIS during the interglacial-like insolation maximum. Although NHSI was as high around 150 ka BP as during the MIS 3 peak at ~55 ka BP, interstadials were weaker and colder during the second half of MIS 6. We propose that the larger continental extent of the EIS ultimately controlled the weaker inland propagation of DO-like temperature changes to the Black Sea region. Overall, we suggest that the spatial extent of the southern and eastern margins of the EIS into the Eurasian continent probably played a crucial role for the propagation of temperature from the North Atlantic toward Eurasia.

Data Availability Statement

The data used in the present study are available online as Supporting Information Data Set S1 and at Zenodo (http://doi.org/10.5281/zenodo.3906001).

References

Arz, H.W., Böttcher, M., Burmeister, C., Dellwig, O., Fisch, K., Hehl, U., et al. (2014). Biological/biogeochemical processes and element fluxes at the Black Sea pelagic redoxcline, sedimentation processes and the Late Holocene development of the system - Cruise MSM33 - November 2 - December 6, 2013 - Cádiz (Spain) - Varna (Bulgaria). MARIA MERIAN Berichte. https://doi.org/10.2312/cr_msm33

Bachmann, O., Schoene, B., Schnyder, C., & Spikings, R. (2010). The ^{40}Ar/^{39}Ar and U/Pb dating of young rhyolites in the Kos-Nisyros volcanic complex, Eastern Aegean Arc, Greece: Age discordance due to excess ^{40}Ar in biotite. *Geochemistry, Geophysics, Geosystems*, *11*, Q0AA08. https://doi.org/10.1029/2010GC003073

Badertscher, S., Fleitmann, D., Cheng, H., Edwards, R. L., Göktürk, O. M., Zumbühl, A., et al. (2011). Pleistocene water intrusions from the Mediterranean and Caspian seas into the Black Sea. *Nature Geoscience*, *4*, 236–239. https://doi.org/10.1038/ngeo1106

Bard, E., Delaygue, G., Rostek, F., Antonioli, F., Silenzi, S., & Schrag, D. P. (2002). Hydrological conditions over the western Mediterranean basin during the deposition of the cold Sapropel 6 (ca. 175 kyr BP). *Earth and Planetary Science Letters*, *202*, 481–494. https://doi.org/10.1016/S0012-821X(02)00788-4

Barker, S., Chen, J., Gong, X., Jonkers, L., Knorr, G., & Thornalley, D. (2015). Icebergs not the trigger for North Atlantic cold events. *Nature*, *520*, 333–336. https://doi.org/10.1038/nature14330

Barker, S., Knorr, G., Edwards, R. L., Parrenin, F., Putnam, A. E., Skinner, L. C., et al. (2011). 800,000 years of abrupt climate variability. *Science*, *334*, 347–351. https://doi.org/10.1126/science.1203580

Batchelor, C. L., Margold, M., Krapp, M., Murton, D. K., Dalton, A. S., Gibbard, P. L., et al. (2019). The configuration of Northern Hemisphere ice sheets through the Quaternary. *Nature Communications*, *10*, 3713. https://doi.org/10.1038/s41467-019-11601-2

Berger, A., & Loutre, M. F. (1991). Insolation values for the climate of the last 10 million years. *Quaternary Science Reviews*, *10*, 297, https://doi.org/10.1016/0277-3791(91)90033-Q–317.

Bintanja, R., & van de Wal, R. S. W. (2008). North American ice-sheet dynamics and the onset of 100,000-year glacial cycles. *Nature*, *454*, 869–872. https://doi.org/10.1038/nature07158

Blaga, C., Reichart, G.-J., Heiri, O., & Sinninghe Damsté, J. (2009). Tetraether membrane lipid distributions in water-column particulate matter and sediments: A study of 47 European lakes along a north–south transect. *Journal of Paleolimnology*, *41*, 523–540. https://doi.org/10.1007/s10933-008-9242-2

Bond, G., Broecker, W., Johnsen, S., McManus, J., Labeyrie, L., Jouzel, J., & Bonani, G. (1993). Correlations between climate records from North Atlantic sediments and Greenland ice. *Nature*, *365*, 143–147. https://doi.org/10.1038/365143a0

Boswell, S. M., Toucanne, S., Pitel-Roudaut, M., Creyts, T. T., Eynaud, F., & Bayon, G. (2019). Enhanced surface melting of the Fennoscandian Ice Sheet during periods of North Atlantic cooling. *Geology*, *47*, 664–668. https://doi.org/10.1130/G46370.1

Çağatay, M. N., Eriş, K. K., Makaroğlu, Ö., Yakupoğlu, N., Henry, P., Leroy, S. A. G., et al. (2019). The Sea of Marmara during Marine Isotope Stages 5 and 6. *Quaternary Science Reviews*, *220*, 124–141. https://doi.org/10.1016/j.quascirev.2019.07.031

Camuera, J., Jiménez-Moreno, G., Ramos-Román, M. J., García-Alix, A., Toney, J. L., Anderson, R. S., et al. (2019). Vegetation and climate changes during the last two glacial-interglacial cycles in the western Mediterranean: A new long pollen record from Padul (southern Iberian Peninsula). *Quaternary Science Reviews*, *205*, 86–105. https://doi.org/10.1016/j.quascirev.2018.12.013

Camuera, J., Jiménez-Moreno, G., Ramos-Román, M. J., García-Alix, A., Toney, J. L., Anderson, R. S., et al. (2018). Orbital-scale environmental and climatic changes recorded in a new ~200,000-year-long multiproxy sedimentary record from Padul, southern Iberian Peninsula. *Quaternary Science Reviews*, *198*, 91–114. https://doi.org/10.1016/j.quascirev.2018.08.014

Castañeda, I. S., & Schouten, S. (2011). A review of molecular organic proxies for examining modern and ancient lacustrine environments. *Quaternary Science Reviews*, *30*, 2851–2891. https://doi.org/10.1016/j.quascirev.2011.07.009

Colleoni, F., Krinner, G., Jakobsson, M., Peyaud, V., & Ritz, C. (2009). Influence of regional parameters on the surface mass balance of the Eurasian ice sheet during the peak Saalian (140 kya). *Global and Planetary Change*, *68*, 132–148. https://doi.org/10.1016/j.gloplacha.2009.03.021

Colleoni, F., Wekerle, C., Näslund, J.-O., Brandefelt, J., & Masina, S. (2016). Constraint on the penultimate glacial maximum Northern Hemisphere ice topography (≈140 kyrs BP). *Quaternary Science Reviews*, *137*, 97–112. https://doi.org/10.1016/j.quascirev.2016.01.024

Cortina, A., Sierro, F. J., Flores, J. A., Martrat, B., & Grimalt, J. O. (2015). The response of SST to insolation and ice sheet variability from MIS 3 to MIS 11 in the northwestern Mediterranean Sea (Gulf of Lions). *Geophysical Research Letters*, *42*, 10,366–310,374. https://doi.org/10.1002/2015GL065539

Dansgaard, W., Johnsen, S. J., Clausen, H. B., Dahl-Jensen, D., Gundestrup, N. S., Hammer, C. U., et al. (1993). Evidence for general instability of past climate from a 250-kyr ice-core record. *Nature*, *364*, 218–220. https://doi.org/10.1038/364218a0

Ehlers, J., & Gibbard, P. L. (2007). The extent and chronology of Cenozoic global glaciation. *Quaternary International*, *164-165*, 6–20. https://doi.org/10.1016/j.quaint.2006.10.008

Emeis, K. C., Schulz, H., Struck, U., Rossignol-Strick, M., Erlenkeuser, H., Howell, M. W., et al. (2003). Eastern Mediterranean surface water temperatures and δ^{18}O composition during deposition of sapropels in the late Quaternary. *Paleoceanography*, *18*(1), 1005. https://doi.org/10.1029/2000PA000617

Feurdean, A., Perşoiu, A., Tanţău, I., Stevens, T., Magyari, E. K., Onac, B. P., et al. (2014). Climate variability and associated vegetation response throughout Central and Eastern Europe (CEE) between 60 and 8 ka. *Quaternary Science Reviews*, *106*, 206–224. https://doi.org/10.1016/j.quascirev.2014.06.003

Fietz, S., Martínez-Garcia, A., Huguet, C., Rueda, G., & Rosell-Melé, A. (2011). Constraints in the application of the Branched and Isoprenoid Tetraether index as a terrestrial input proxy. *Journal of Geophysical Research*, *116*, C10032. https://doi.org/10.1029/2011JC007062

Fleitmann, D., Cheng, H., Badertscher, S., Edwards, R. L., Mudelsee, M., Göktürk, O. M., et al. (2009). Timing and climatic impact of Greenland interstadials recorded in stalagmites from northern Turkey. *Geophysical Research Letters*, *36*, L19707. https://doi.org/10.1029/2009GL040050

Ganopolski, A., & Rahmstorf, S. (2001). Rapid changes of glacial climate simulated in a coupled climate model. *Nature*, *409*, 153–158. https://doi.org/10.1038/35051500

Grant, K. M., Rohling, E. J., Bar-Matthews, M., Ayalon, A., Medina-Elizalde, M., Ramsey, C. B., et al. (2012). Rapid coupling between ice volume and polar temperature over the past 150,000 years. *Nature*, *491*, 744–747. https://doi.org/10.1038/nature11593

Heinrich, H. (1988). Origin and consequences of cyclic ice rafting in the Northeast Atlantic Ocean during the past 130,000 years. *Quaternary Research*, *29*, 142–152. https://doi.org/10.1016/0033-5894(88)90057-9

Hopmans, E. C., Schouten, S., & Sinninghe Damsté, J. S. (2016). The effect of improved chromatography on GDGT-based palaeoproxies. *Organic Geochemistry*, *93*, 1–6. https://doi.org/10.1016/j.orggeochem.2015.12.006

Hopmans, E. C., Weijers, J. W. H., Schefuß, E., Herfort, L., Sinninghe Damsté, J. S., & Schouten, S. (2004). A novel proxy for terrestrial organic matter in sediments based on branched and isoprenoid tetraether lipids. *Earth and Planetary Science Letters*, *224*, 107–116. https://doi.org/10.1016/j.epsl.2004.05.012

Hughes, P. D., & Gibbard, P. L. (2018). Global glacier dynamics during 100 ka Pleistocene glacial cycles. *Quaternary Research*, *90*, 222–243. https://doi.org/10.1017/qua.2018.37

Hurley, S. J., Elling, F. J., Könneke, M., Buchwald, C., Wankel, S. D., Santoro, A. E., et al. (2016). Influence of ammonia oxidation rate on thaumarchaeal lipid composition and the TEX$_{86}$ temperature proxy. *Proceedings of the National Academy of Sciences of the United States of America*, *113*, 7762–7767. https://doi.org/10.1073/pnas.1518534113

Kaiser, J., & Arz, H. W. (2016). Sources of sedimentary biomarkers and proxies with potential paleoenvironmental significance for the Baltic Sea. *Continental Shelf Research*, *122*, 102–119. https://doi.org/10.1016/j.csr.2016.03.020

Koltai, G., Spötl, C., Shen, C. C., Wu, C. C., Rao, Z., Palcsu, L., et al. (2017). A penultimate glacial climate record from southern Hungary. *Journal of Quaternary Science*, *32*, 946–956. https://doi.org/10.1002/jqs.2968

Kusch, S., Rethemeyer, J., Hopmans, E. C., Wacker, L., & Mollenhauer, G. (2016). Factors influencing ^{14}C concentrations of algal and archaeal lipids and their associated sea surface temperature proxies in the Black Sea. *Geochimica et Cosmochimica Acta*, *188*, 35–57. https://doi.org/10.1016/j.gca.2016.05.025

Kwiecien, O., Stockhecke, M., Pickarski, N., Heumann, G., Litt, T., Sturm, M., et al. (2014). Dynamics of the last four glacial terminations recorded in Lake Van, Turkey. *Quaternary Science Reviews*, *104*, 42–52. https://doi.org/10.1016/j.quascirev.2014.07.001

Lambeck, K. (1996). Limits on the areal extent of the Barents Sea ice sheet in Late Weichselian time. *Global and Planetary Change*, *12*, 41–51. https://doi.org/10.1016/0921-8181(95)00011-9

Lambeck, K., Purcell, A., Funder, S., Kjær, K. H., Larsen, E., & Moller, P. (2006). Constraints on the Late Saalian to early Middle Weichselian ice sheet of Eurasia from field data and rebound modelling. *Boreas*, *35*, 539–575. https://doi.org/10.1080/03009480600781875

Larsen, E., Kjær, K., Demidov, I., Funder, S., Grøsfjeld, K., Houmark-Nielsen, M., et al. (2006). Late Pleistocene glacial and lake history of northwestern Russia. *Boreas*, *35*, 394–424. https://doi.org/10.1080/03009480600781958

Laskar, J., Robutel, P., Joutel, F., Gastineau, M., Correia, A. C. M., & Levrard, B. (2004). A long-term numerical solution for the insolation quantities of the Earth. *Astronomy & Astrophysics*, *428*, 261–285. https://doi.org/10.1051/0004-6361:20041335

Lisiecki, L.E. & Raymo, M.E. (2005). A Pliocene-Pleistocene stack of 57 globally distributed benthic δ^{18}O records. Paleoceanography 20. https://doi.org/10.1029/2004PA001071

Margari, V., Skinner, L. C., Hodell, D. A., Martrat, B., Toucanne, S., Grimalt, J. O., et al. (2014). Land-ocean changes on orbital and millennial time scales and the penultimate glaciation. *Geology*, *42*, 183–186. https://doi.org/10.1130/G35070.1

Margari, V., Skinner, L. C., Tzedakis, P. C., Ganopolski, A., Vautravers, M., & Shackleton, N. J. (2010). The nature of millennial-scale climate variability during the past two glacial periods. *Nature Geoscience*, *3*, 127–131. https://doi.org/10.1038/ngeo740

Marks, L., Karabanov, A., Nitychoruk, J., Bahdasarau, M., Krzywicki, T., Majecka, A., et al. (2018). Revised limit of the Saalian ice sheet in central Europe. *Quaternary International*, *478*, 59–74. https://doi.org/10.1016/j.quaint.2016.07.043

Martrat, B., Grimalt, J. O., Lopez-Martinez, C., Cacho, I., Sierro, F. J., Flores, J. A., et al. (2004). Abrupt temperature changes in the Western Mediterranean over the past 250,000 years. *Science*, *306*, 1762–1765. https://doi.org/10.1126/science.1101706

Martrat, B., Grimalt, J. O., Shackleton, N. J., de Abreu, L., Hutterli, M. A., & Stocker, T. F. (2007). Four climate cycles of recurring deep and surface water destabilizations on the Iberian margin. *Science*, *317*, 502–507. https://doi.org/10.1126/science.1139994

McManus, J. F., Oppo, D. W., & Cullen, J. L. (1999). A 0.5-million-year record of millennial-scale climate variability in the North Atlantic. *Science*, *283*, 971–975. https://doi.org/10.1126/science.283.5404.971

Ménot, G., & Bard, E. (2012). A precise search for drastic temperature shifts of the past 40,000 years in southeastern Europe. *Paleoceanography*, *27*, PA2210. https://doi.org/10.1029/2012PA002291

North Greenland Ice Core Project members, Andersen, K. K., Azuma, N., Barnola, J. M., Bigler, M., Biscaye, P., Caillon, N., et al. (2004). High-resolution record of Northern Hemisphere climate extending into the last interglacial period. *Nature*, *431*, 147–151. https://doi.org/10.1038/nature02805

Nowaczyk, N. R., Arz, H. W., Frank, U., Kind, J., & Plessen, B. (2012). Dynamics of the Laschamp geomagnetic excursion from Black Sea sediments. *Earth and Planetary Science Letters*, *351-352*, 54–69. https://doi.org/10.1016/j.epsl.2012.06.050

Ön, Z. B., & Özeren, M. S. (2018). Temperature and precipitation variability in eastern Anatolia: Results from independent component analysis of Lake Van sediment data spanning the last 250 kyr BP. *Quaternary International*, *514*, 119–129. https://doi.org/10.1016/j.quaint.2018.11.037

Penaud, A., Eynaud, F., Turon, J. L., Zaragosi, S., Malaizé, B., Toucanne, S., & Bourillet, J. F. (2009). What forced the collapse of European ice sheets during the last two glacial periods (150 ka B.P. and 18 ka cal B.P.)? Palynological evidence. *Palaeogeography, Palaeoclimatology, Palaeoecology*, *281*, 66–78. https://doi.org/10.1016/j.palaeo.2009.07.012

Pollard, D., & Barron, E. J. (2003). Causes of model-data discrepancies in European climate during oxygen isotope stage 3 with insights from the last glacial maximum. *Quaternary Research*, *59*, 108–113. https://doi.org/10.1016/S0033-5894(02)00019-4

Powers, L., Werne, J. P., Vanderwoude, A. J., Sinninghe Damste, J. S., Hopmans, E. C., & Schouten, S. (2010). Applicability and calibration of the TEX$_{86}$ paleothermometer in lakes. *Organic Geochemistry*, *41*, 404–413. https://doi.org/10.1016/j.orggeochem.2009.11.009

Qin, W., Carlson, L. T., Armbrust, E. V., Devol, A. H., Moffett, J. W., Stahl, D. A., & Ingalls, A. E. (2015). Confounding effects of oxygen and temperature on the TEX$_{86}$ signature of marine Thaumarchaeota. *Proceedings of the National Academy of Sciences*, *112*, 10,979–10,984. https://doi.org/10.1073/pnas.1501568112

Randlett, M. È., Coolen, M. J. L., Stockhecke, M., Pickarski, N., Litt, T., Balkema, C., et al. (2014). Alkenone distribution in Lake Van sediment over the last 270 ka: Influence of temperature and haptophyte species composition. *Quaternary Science Reviews*, *104*, 53–62. https://doi.org/10.1016/j.quascirev.2014.07.009

Rohling, E. J., Marino, G., & Grant, K. M. (2015). Mediterranean climate and oceanography, and the periodic development of anoxic events (sapropels). *Earth Science Reviews*, *143*, 62e97. https://doi.org/10.1016/j.earscirev.2015.01.008

Roucoux, K. H., Tzedakis, P. C., Lawson, I. T., & Margari, V. (2011). Vegetation history of the penultimate glacial period (Marine isotope stage 6) at Ioannina, north-west Greece. *Journal of Quaternary Science*, *26*, 616–626. https://doi.org/10.1002/jqs.1483

Rousseau, D. D., Antoine, P., Boers, N., Lagroix, F., Ghil, M., Lomax, J., et al. (2020). Dansgaard–Oeschger-like events of the penultimate climate cycle: The loess point of view. *Climate of the Past*, *16*, 713–727. https://doi.org/10.5194/cp-16-713-2020

Savitzky, A., & Golay, M. J. E. (1964). Smoothing and differentiation of data by simplified least squares procedures. *Analytical Chemistry*, *36*, 1627–1639. https://doi.org/10.1021/ac60214a047

Schmidt, F., Hinrichs, K.-U., & Elvert, M. (2010). Sources, transport, and partitioning of organic matter at a highly dynamic continental margin. *Marine Chemistry*, *118*, 37–55. https://doi.org/10.1016/j.marchem.2009.10.003

Schmiedl, G., Mitschele, A., Beck, S., Emeis, K. C., Hemleben, C., Schulz, H., et al. (2003). Benthic foraminiferal record of ecosystem variability in the eastern Mediterranean Sea during times of sapropel S5 and S6 deposition. *Palaeogeography, Palaeoclimatology, Palaeoecology*, *190*, 139–164. https://doi.org/10.1016/S0031-0182(02)00603-X

Schmitt, A. K., Danišík, M., Evans, N. J., Siebel, W., Kiemele, E., Aydin, F., & Harvey, J. C. (2011). Acigöl rhyolite field, Central Anatolia (part 1): High-resolution dating of eruption episodes and zircon growth rates. *Contributions to Mineralogy and Petrology*, *162*, 1215–1231. https://doi.org/10.1007/s00410-011-0648-x

Schouten, S., Hopmans, E. C., Schefuß, E., & Sinninghe Damsté, J. S. (2002). Distributional variations in marine crenarchaeotal membrane lipids: A new tool for reconstructing ancient sea water temperatures? *Earth and Planetary Science Letters*, *204*, 265–274. https://doi.org/10.1016/S0012-821X(02)00979-2

Schouten, S., Hopmans, E. C., & Sinninghe Damsté, J. S. (2013). The organic geochemistry of glycerol dialkyl glycerol tetraether lipids: A review. *Organic Geochemistry*, *54*, 19–61. https://doi.org/10.1016/j.orggeochem.2012.09.006

Shumilovskikh, L. S., Arz, H. W., Wegwerth, A., Fleitmann, D., Marret, F., Nowaczyk, N., et al. (2013). Vegetation and environmental changes in Northern Anatolia between 134 and 119 ka recorded in Black Sea sediments. *Quaternary Research*, *80*, 349–360. https://doi.org/10.1016/j.yqres.2013.07.005

Sinopoli, G., Peyron, O., Masi, A., Holtvoeth, J., Francke, A., Wagner, B., & Sadori, L. (2019). Pollen-based temperature and precipitation changes in the Ohrid Basin (western Balkans) between 160 and 70 ka. *Climate of the Past*, *15*, 53–71. https://doi.org/10.5194/cp-15-53-2019

Smith, P. E., York, D., Chen, Y., & Evensen, N. M. (1996). Single crystal ^{40}Ar-^{39}Ar dating of a Late Quaternary paroxysm on Kos, Greece: Concordance of terrestrial and marine ages. *Geophysical Research Letters*, *23*, 3047–3050. https://doi.org/10.1029/96GL02759

Smith, R. W., Bianchi, T. S., & Li, X. (2012). A re-evaluation of the use of branched GDGTs as terrestrial biomarkers: Implications for the BIT index. *Geochimica et Cosmochimica Acta*, *80*, 14–29. https://doi.org/10.1016/j.gca.2011.11.025

Soulet, G., Ménot, G., Garreta, V., Rostek, F., Zaragosi, S., Lericolais, G., & Bard, E. (2011). Black Sea "Lake" reservoir age evolution since the Last Glacial—Hydrologic and climatic implications. *Earth and Planetary Science Letters*, *308*, 245–258. https://doi.org/10.1016/j.epsl.2011.06.002

Stockhecke, M., Sturm, M., Brunner, I., Schmincke, H. U., Sumita, M., Kipfer, R., et al. (2014). Sedimentary evolution and environmental history of Lake Van (Turkey) over the past 600 000 years. *Sedimentology*, *61*, 1830–1861. https://doi.org/10.1111/sed.12118

Stockhecke, M., Timmermann, A., Kipfer, R., Haug, G. H., Kwiecien, O., Friedrich, T., et al. (2016). Millennial to orbital-scale variations of drought intensity in the Eastern Mediterranean. *Quaternary Science Reviews*, *133*, 77–95. https://doi.org/10.1016/j.quascirev.2015.12.016

Svendsen, J. I., Alexanderson, H., Astakhov, V. I., Demidov, I., Dowdeswell, J. A., Funder, S., et al. (2004). Late Quaternary ice sheet history of northern Eurasia. *Quaternary Science Reviews*, *23*, 1229–1271. https://doi.org/10.1016/j.quascirev.2003.12.008

Toucanne, S., Zaragosi, S., Bourillet, J. F., Cremer, M., Eynaud, F., van Vliet-Lanoë, B., et al. (2009). Timing of massive 'Fleuve Manche' discharges over the last 350 kyr: Insights into the European ice-sheet oscillations and the European drainage network from MIS 10 to 2. *Quaternary Science Reviews*, *28*, 1238–1256. https://doi.org/10.1016/j.quascirev.2009.01.006

Turich, C., Freeman, K. H., Bruns, M. A., Conte, M., Jones, A. D., & Wakeham, S. G. (2007). Lipids of marine Archaea: Patterns and provenance in the water-column and sediments. *Geochimica et Cosmochimica Acta*, *71*, 3272–3291. https://doi.org/10.1016/j.gca.2007.04.013

Tzedakis, P. C., Frogley, M. R., Lawson, I. T., Preece, R. C., Cacho, I., & de Abreu, L. (2004). Ecological thresholds and patterns of millennial-scale climate variability: The response of vegetation in Greece during the last glacial period. *Geology*, *32*, 109–112. https://doi.org/10.1130/G20118.1

Tzedakis, P. C., McManus, J. F., Hooghiemstra, H., Oppo, D. W., & Wijmstra, T. A. (2003). Comparison of changes in vegetation in northeast Greece with records of climate variability on orbital and suborbital frequencies over the last 450 000 years. *Earth and Planetary Science Letters*, *212*, 197–212. https://doi.org/10.1016/S0012-821X(03)00233-4

Van Meerbeeck, C. J., Renssen, H., Roche, D. M., Wohlfarth, B., Bohncke, S. J. P., Bos, J. A. A., et al. (2011). The nature of MIS 3 stadial-interstadial transitions in Europe: New insights from model-data comparisons. *Quaternary Science Reviews*, *30*, 3618–3637. https://doi.org/10.1016/j.quascirev.2011.08.002

Wainer, K., Genty, D., Blamart, D., Bar-Matthews, M., Quinif, Y., & Plagnes, V. (2013). Millennial climatic instability during penultimate glacial period recorded in a south-western France speleothem. *Palaeogeography, Palaeoclimatology, Palaeoecology*, *376*, 122–131. https://doi.org/10.1016/j.palaeo.2013.02.026

Wang, Y., Cheng, H., Edwards, R. L., Kong, X., Shao, X., Chen, S., et al. (2008). Millennial- and orbital-scale changes in the East Asian monsoon over the past 224,000 years. *Nature*, *451*, 1090–1093. https://doi.org/10.1038/nature06692

Wegwerth, A., Dellwig, O., Kaiser, J., Ménot, G., Bard, E., Shumilovskikh, L., et al. (2014). Meltwater events and the Mediterranean reconnection at the Saalian–Eemian transition in the Black Sea. *Earth and Planetary Science Letters*, *404*, 124–135. https://doi.org/10.1016/j.epsl.2014.07.030

Wegwerth, A., Dellwig, O., Wulf, S., Plessen, B., Kleinhanns, I. C., Nowaczyk, N. R., et al. (2019). Major hydrological shifts in the Black Sea "Lake" in response to ice sheet collapses during MIS 6 (130–184 ka BP). *Quaternary Science Reviews*, *219*, 126–144. https://doi.org/10.1016/j.quascirev.2019.07.008

Wegwerth, A., Eckert, S., Dellwig, O., Schnetger, B., Severmann, S., Weyer, S., et al. (2018). Redox evolution during Eemian and Holocene sapropel formation in the Black Sea. *Palaeogeography Palaeoclimatology Palaeoecology*, *489*, 249–260. https://doi.org/10.1016/j.palaeo.2017.10.014

Wegwerth, A., Ganopolski, A., Ménot, G., Kaiser, J., Dellwig, O., Bard, E., et al. (2015). Black Sea temperature response to glacial millennial-scale climate variability. *Geophysical Research Letters*, *42*, 8147–8154. https://doi.org/10.1002/2015GL065499

Wegwerth, A., Kaiser, J., Dellwig, O., Shumilovskikh, L. S., Nowaczyk, N. R., & Arz, H. W. (2016). Northern hemisphere climate control on the environmental dynamics in the glacial Black Sea "Lake". *Quaternary Science Reviews*, *135*, 41–53. https://doi.org/10.1016/j.quascirev.2016.01.016

Weijers, J. W. H., Schouten, S., Spaargaren, O. C., & Sinninghe Damsté, J. S. (2006). Occurrence and distribution of tetraether membrane lipids in soils: Implications for the use of the TEX$_{86}$ proxy and the BIT index. *Organic Geochemistry*, *37*, 1680–1693. https://doi.org/10.1016/j.orggeochem.2006.07.018

Zhang, X., Prange, M., Merkel, U., & Schulz, M. (2014). Instability of the Atlantic overturning circulation during marine isotope stage 3. *Geophysical Research Letters*, *41*, 4285–4293. https://doi.org/10.1002/2014GL060321

Zhang, Y. G., Zhang, C. L., Liu, X.-L., Li, L., Hinrichs, K.-U., & Noakes, J. E. (2011). Methane Index: A tetraether archaeal lipid biomarker indicator for detecting the instability of marine gas hydrates. *Earth and Planetary Science Letters*, *307*, 525–534. https://doi.org/10.1016/j.epsl.2011.05.031

Zubakov, V. A. (1988). Climatostratigraphic scheme of the Black Sea Pleistocene and its correlation with the oxygen-isotope scale and glacial events. *Quaternary Research*, *29*, 1–24. https://doi.org/10.1016/0033-5894(88)90067-1